Thermal Modeling of a SOFC Stack for Maritime and Heavy-Duty Transport Applications

1st Takarli Zineb
UMLP, CNRS
Institut FEMTO-ST
Belfort, France
zineb.takarli@femto-st.fr

2nd Pera Marie Cecile
UMLP, CNRS
Institut FEMTO-ST
Belfort, France
marie-cecile.pera@umlp.fr

3rd Chrenko Daniela
UMLP, CNRS
Institut FEMTO-ST
Belfort, France
Daniela.chrenko@utbm.fr

4th Jaafar Amine
Université de Toulouse, CNRS
Institut Laplace
Toulouse, France
Jaafar@laplace.univ-tlse.fr

5th Turpin Christophe
Université de Toulouse, CNRS
Institut Laplace
Toulouse, France
Turpin@laplace.univ-tlse.fr

***Abstract*— Solid Oxide Fuel Cells (SOFCs) are promising candidates for maritime and heavy-duty transport applications due to their high efficiency and fuel flexibility. However, their high operating temperature makes thermal management a critical issue for performance, durability, and system integration.**

In this work, a two-dimensional thermal model of a planar SOFC stack is developed to predict temperature evolution within the different stack layers and to locate the main heat sources during operation. The model includes conductive, convective, mass transport and radiative heat transfer, together with internal heat generation related to cell operation. Temperature evolution is analyzed at several locations under representative operating conditions. The results provide insight into the thermal distribution within the stack and the dominant thermal phenomena governing its behavior. This work is part of a broader multiphysics modeling framework of SOFC systems.

Keywords*— *Solid Oxide Fuel Cell, thermal model, electro-thermal analogy, nodal modeling, heat sources, temperature evolution, stack thermal behavior.

I. INTRODUCTION

Solid Oxide Fuel Cells (SOFCs) are considered promising energy conversion systems for applications requiring high efficiency, fuel flexibility, and long operating durations, such as maritime transport [1] and heavy-duty transport [2]. Recent industrial developments also highlight the growing interest in fuel cell technologies for maritime applications [3]. In these sectors, the demand for efficient and low-emission power systems is continuously increasing, making fuel cell technologies attractive alternatives to conventional energy conversion systems. Among them, SOFCs offer significant potential due to their high electrical efficiency and their ability to operate with a variety of fuels.

Another major advantage of SOFC systems lies in the high amount of thermal energy released during operation. This heat can potentially be recovered and reused at the system level, there by improving the overall energy efficiency. Such a feature is particularly relevant for heavy-duty and maritime applications, where energy recovery and global system efficiency are key considerations. However, the high operating temperature of SOFCs also makes thermal management a key aspect of their operation. Temperature levels and thermal gradients strongly affect stack performance, durability, mechanical integrity, and safe operation.

In this context, thermal modeling becomes an essential tool for analyzing the heat transfer mechanisms occurring within the stack and for predicting the temperature evolution in its different layers. It also helps identify the main heat sources generated during operation and provides useful insight for improving thermal management strategies. Moreover, stack-level thermal modeling constitutes a first step toward the future development of a complete thermal model of the overall SOFC system, including heat recovery considerations.

This work is part of a multiphysics modeling framework of a planar SOFC stack operating with pure hydrogen and gas mixtures. This paper focuses on the development of a two-dimensional thermal model to predict the temperature behavior within the stack and identify the dominant thermal phenomena. Numerical simulations are performed to analyze the temperature evolution at several locations of the stack.

The remainder of this paper is organized as follows. First, the SOFC technology and its operating principle are briefly introduced. Then, the proposed thermal model based on an electrical analogy is presented, followed by the nodal energy balance formulation. The different heat fluxes and internal heat sources considered in the model are subsequently described. The complete two-dimensional thermal model is then detailed. Finally, the simulation results are presented and discussed, and the model is validated against experimental data available in the literature for the same SOFC stack (Elcogen E350).

A. Components and operating principle of a SOFC

A SOFC cell is composed of four main components: the anode, the solid electrolyte, the cathode, and the interconnects.

The anode is supplied with a fuel, such as hydrogen or a gaseous mixture derived from biofuels or industrial process by-products like (CH_4, NH_3, CO, CO_2, etc.), whereas the cathode is fed with air as the oxidant [4]. Fig. 1

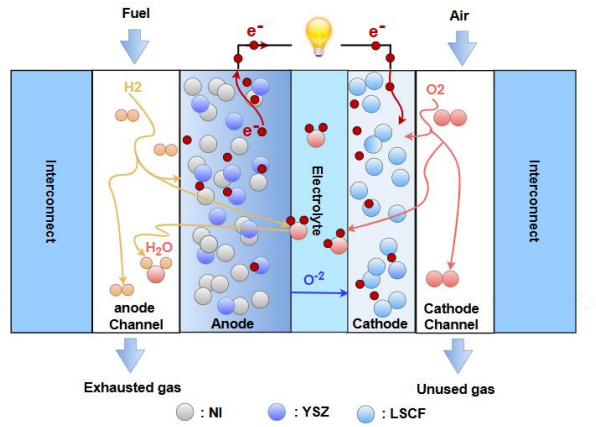


Fig. 1. Operating principle of the SOFC stack

The operating principle of a SOFC is based on the reduction of oxygen at the cathode into O^{2-} ions, which migrate through the electrolyte due to its ionic conductivity at high temperature. These ions then react with the fuel at the anode. This electrochemical reaction produces oxidation products and releases electrons, which flow through an external circuit, thereby generating electrical power.

B. Studied SOFC Stack

The experimental investigations were carried out on an Elcogen E350 planar SOFC stack [5] [6] as shown in Fig. 2. This stack is composed of 15 unit cells and delivers a rated power of 350 W. According to the manufacturer's technical data, its maximum open-circuit voltage under hydrogen is 18 V, while the minimum operating voltage is 10 V. The nominal current is 30 A. The stack is also characterized by a maximum fuel utilization of 0.7 and an air utilization range of 0.12–0.3 under nominal current conditions. Owing to these characteristics, the Elcogen E350 stack constitutes a relevant experimental platform for the thermal analysis and validation of the proposed model.

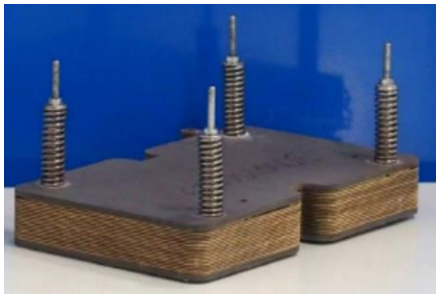


Fig. 2. Elcogen E350 SOFC stack

II. THERMAL MODEL

The thermal model is based on an electro-thermal analogy [7], in which temperature is treated as an electrical potential and heat flow as an electrical current. Fig. 3 and Table I.

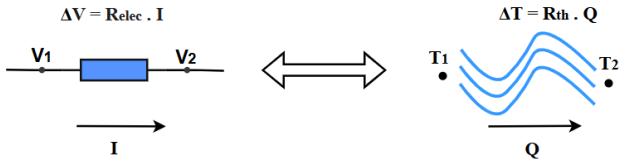


Fig. 3. Electro-thermal analogy between electrical and thermal domaines

TABLE I. ELECTRO-THERMAL ANALOGY

Domain	Effort	Flow
Electrical	Voltage V	Current I
Thermal	Temperature T	Heat flow Q

Using this approach, the thermal behavior of the stack is represented by an equivalent nodal network in Fig. 4 composed of thermal resistances, thermal capacitances, and heat sources.

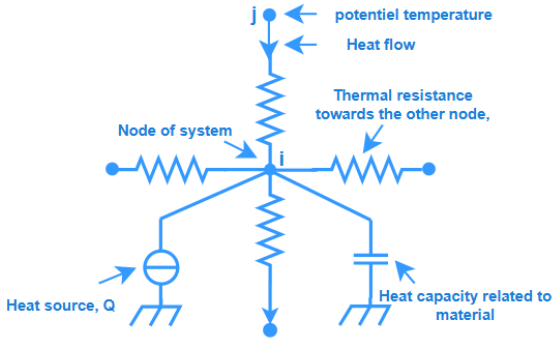


Fig. 4. Equivalent thermal node in the electro-thermal network

From a physical point of view, thermal resistance describes the opposition to heat transfer between two parts of the system, while thermal capacitance represents the ability of a material or component to store thermal energy and thus reflects its thermal inertia. Heat sources account for the thermal energy generated within the stack during operation and are responsible for local temperature rise [7] [8].

The stack is described as a set of interconnected thermal nodes, each associated with a local temperature and linked to neighboring nodes through equivalent thermal elements.

A. Nodal Energy Balance Equation

For each node of the thermal network, an energy balance is established [9] by considering heat storage, heat exchanges with adjacent nodes, and internal heat generation (1).

$$C_{th,i}\frac{dT_i}{dt} = \sum_i \frac{T_j - T_i}{R_{ij}} + Q_i \qquad (1)$$

where $C_{th,i}$ is the thermal capacitance of node i [J/K], T_i and T_j are the temperatures of nodes i and j, respectively [K], R_{ij} is the thermal resistance between nodes i and j [K/W], t is time [s], and Q_i is the heat source term associated with node i [W].

B. Heat flux

1) ***Conductive heat flow*****:** heat transferred through a solid material due to a temperature gradient. (2)

$$Q_{cond} = \frac{\lambda S}{e} * \Delta T \quad (2)$$

$$R_{cond} = \frac{e}{\lambda S} \quad (3)$$

where e is the thickness of the considered layer [m], λ is the thermal conductivity of the material [W\m\K), and [S] is the heat transfer surface area [m²].

2) ***Convective heat flow:*** heat exchanged between a solid surface and a surrounding fluid *[9]*. (4)

$$Q_{conv} = h * S * \Delta T \quad (4)$$

$$R_{conv} = h * S \quad (5)$$

where *h* is the convective heat transfer coefficient [W/m/K].

3) ***Radiative heat flow:*** heat transferred by thermal radiation between a surface and its environment *[9]*. (6)

$$Q_{rad} = F * \varepsilon * \sigma * \left(T_i^4 - T_j^4\right) \quad (6)$$

$$R_{rad} = \frac{1}{F * \varepsilon * \sigma * (T_i^2 + T_j^2) * (T_i + T_j)} \quad (7)$$

where *F* is the view factor between the radiating surfaces (dimensionless), σ is the Stefan–Boltzmann constant ($5.67*10^{-8}$) (W.m-2.K-4).

4) ***Mass transport heat flow:*** heat associated with species transport effects, which may influence local concentration and thermal behavior within the stack *[10]*. (8)

$$Q_{mf} = \dot{m} * cp * \Delta T \quad (8)$$

$$R_{mf} = \frac{1}{\dot{m}\, cp} \quad (9)$$

$\dot{m}$ denotes the mass flow rate [kg/s], and *cp* is the specific heat capacity at constant pressure [J/kg/ K].

C. Heat sources

Due to the different electrochemical and transport phenomena occurring in the anode, electrolyte, and cathode, heat generation is not uniformly distributed within the SOFC stack. The local heat source terms therefore depend on the considered layer and on the underlying physical mechanisms [4] [10] [11] [12].

1) Anode

The heat sources considered in the anode include the heat generated by water formation, the heat associated with mass diffusion phenomena, and the ohmic heat generation. These contributions are considered in the thermal model [4] [9]. (10)

$$Q_a = Q_{c_dif} + Q_{a_ohm} + Q_f \quad (10)$$

$$Q_f = \frac{\Delta S * I * T}{2F} \quad (11)$$

ΔS denotes the entropy change associated with the electrochemical reaction [J /mol/ K], *I* is the electric current [A], *F* is the Faraday constant [96485 C /mol], and the factor *2* corresponds to the number of electrons exchanged in the reaction.

As the associated diffusion overpotential is higher on the anode side, the heat generated by diffusion phenomena is assumed to be primarily localized in the anode [6]. This assumption is also consistent with the anode-supported configuration of the considered SOFC.

$$Q_{a_dif} = \eta_{c_dif} * I \quad (12)$$

$$Q_{a_{ohm}} = R_a * I^2 \quad (13)$$

ηc_dif denotes the diffusion overpotential [V], R_a is the anodic resistance [Ω],

$$R_a = \frac{S}{e_a * \sigma_{a_ion}} + \frac{S}{e_c * \sigma_{c_elec}} \quad (14)$$

e_a is the anode thickness [m], σ_{a_ion} and σ_{a_ion} are the ionic and electronic conductivities, respectively [S/m].

2) Electrolyte

In the electrolyte, the heat generation term is solely associated with ionic ohmic resistance. (15)

$$Q_{e_ohm} = R_{e_ion} * I^2 \quad (15)$$

R_{e_ion} denotes the ionic resistance of the electrolyte (YSZ).

$$R_{e_ion} = \frac{S}{e_e * \sigma_{e_ion}} \quad (16)$$

e_e represents the thickness of the electrolyte [m], and σ its ionic conductivity (S/m).

3) Cathode

At the cathode, since activation overpotentials are predominant, the heat generated by activation losses is assumed to be entirely localized at the cathode [6]. Ohmic heat generation is also considered at the cathode. (17)

$$Q_c = Q_{c_act} + Q_{c_ohm} \quad (17)$$

$$Q_{c_act} = \eta_{c_act} * I \quad (18)$$

$$Q_{c_ohm} = R_c * I^2 \quad (19)$$

η_act denotes the activation overpotential [V], Rc is the cathodic resistance [Ω].

$$R_c = \frac{S}{e_c * \sigma_{c_ion}} + \frac{S}{e_c * \sigma_{c_elec}}$$

e_c represents the thickness of the cathode [m], σ_{c_ion} and σ_{c_ion} are the ionic and electronic conductivities, respectively [S/m].

D. Detailed 2D model

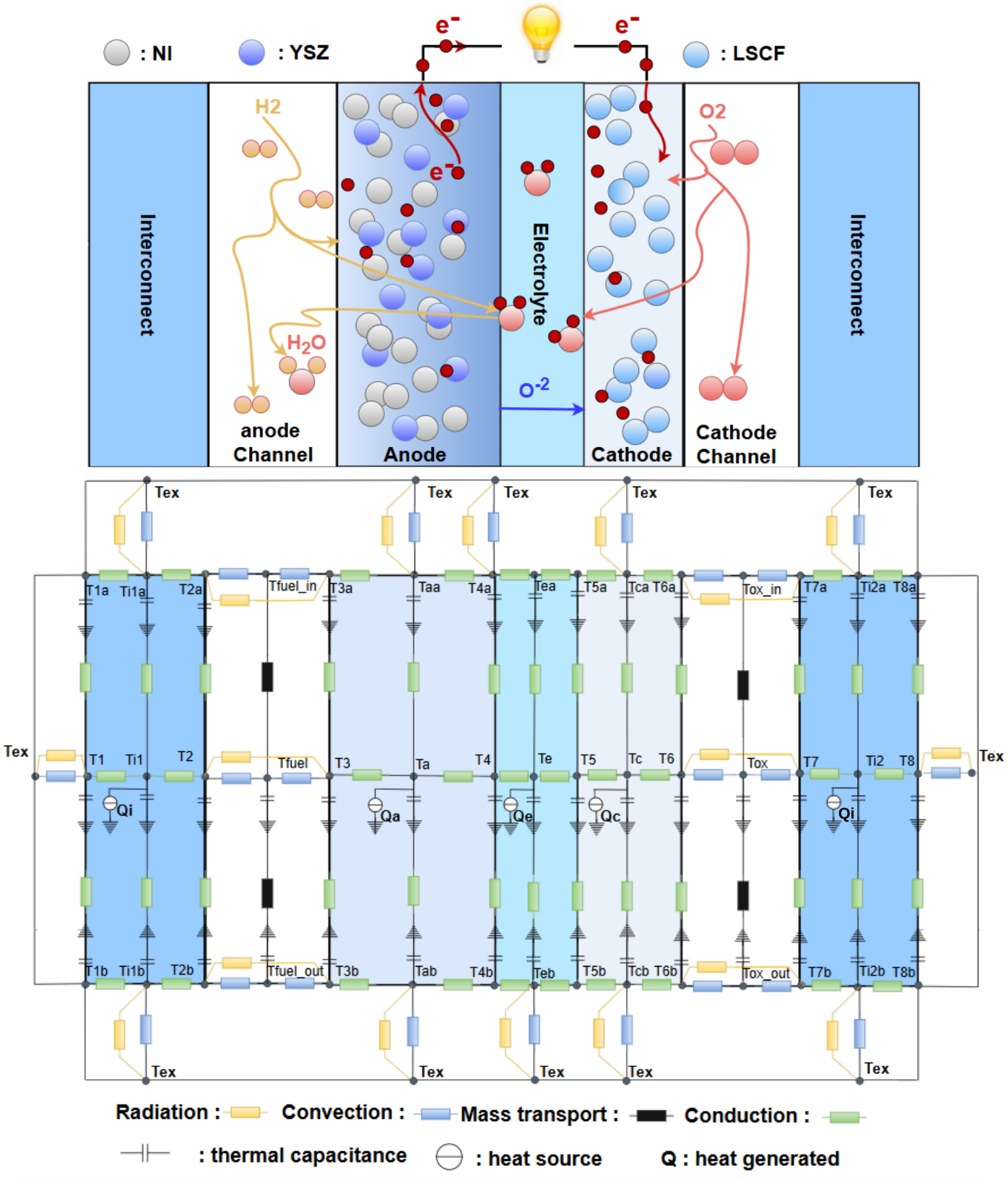


Fig. 5. Detailed 2D thermal model with and localized heat sources.

The developed thermal model represents the SOFC stack in Fig. 5 as a two-dimensional multilayer structure composed of seven main layers: interconnect, anode channel, anode, electrolyte, cathode, cathode channel, and interconnect. It is intended to describe the temperature distribution within the stack by considering the temperature at the center of each layer as well as at both ends in the vertical and horizontal directions. More specifically, the temperature of each layer is represented by the central node located at the middle of the layer. The temperature between two adjacent layers is represented by the intermediate node located at their interface, while the thermal interaction between the stack and the furnace is represented by the node located between the boundary layer and the furnace. The vertical thermal links account for the thermal interaction with the furnace, whereas the horizontal links represent the thermal coupling between adjacent stack layers. The model also includes the different internal heat sources and their localization within the stack according to the underlying physical phenomena.

III. Simulation Results

The developed thermal model was simulated under representative operating conditions. The thermophysical properties and geometrical dimensions of the materials and gases used in the thermal model are listed in Table II and the ionic and electronic conductivities of the stack components are listed in Table III.

TABLE II. Thermophysical Properties of Common Electrode and Electrolyte and Gaz Used. [4] [6] [7]

Layers	C_p (J.kg^{-1}.K^{-1})	λ (J.Kg^{-1}.K^{-1})	ρ (kg.m^{-3})	e (mm)
Anode (Ni/YSZ)	390	6.23	6870	400.10^{-3}
Electrolyte (YSZ)	525	2.57	6086	12.10^{-3}
Cathode LSCF	430	6	3030	5.10^{-3}
Interconect	600	25	7700	2
H_2 (anode chanel)	14870	-	0.0263	0.5-1.5
Air (cathode chanel)	1125	-	0.38	0.5-1.5

TABLE III. Conductivity Parameters. [10] [13]

Layer	σ_{ion} (S.m^{-1})	σ_{elec} (S.m^{-1})
Anode (Ni/YSZ)	$3.34.10^4.e^{(-\frac{10300}{T})}$	$\frac{9.5*10^7}{T}.e^{(-\frac{1150}{T})}$
Electrolyte (YSZ)	$3.34.10^4.e^{(-\frac{10300}{T})}$	-
Cathode LSCF	$\frac{100}{T}.10^{2.51289}+\frac{3036.75}{T}$	$\frac{100}{T}.10^{4.32576}+\frac{15.2}{T}$
Interconect Ferritic steel	-	$200.e^{(-\frac{693.14}{T})}$

A linearly increasing current is applied to the stack over an active surface area of 121 cm², ramping from 0 A to 35 A over a period of 0.6 h at 923 K .The simulation results are compared to experimental measurements obtained from the ELCOGEN stack operating at 923 K [6]. As illustrated in Fig. 6, the model accurately reproduces the dynamic thermal behavior of the stack at the inlet and outlet of both the anodic and cathodic compartments, showing good agreement with the experimentally measured temperature trends for the fuel inlet and outlet temperatures T_{fuel_in}, T_{fuel_out} as well as the air inlet and outlet temperatures T_{ox_in}, T_{ox_out}. The temperature variation ΔT predicted by the model is consistent with the measured data throughout the current ramp, confirming the model's ability to capture the transient response of the stack. However, a discrepancy is observed between the absolute temperature values predicted by the model and those measured experimentally. This deviation is primarily attributed to two simplifying assumptions adopted in the present model. First, all nodal temperatures are initialized uniformly at 923 K, whereas the experimental stack may exhibit non-uniform temperature distributions at the start of the measurement. Second, the inlet temperatures T_in of both the fuel and air streams are held constant at 923 K in the model, while experimentally they are not strictly constant and are already slightly above this reference value prior to the application of the current.

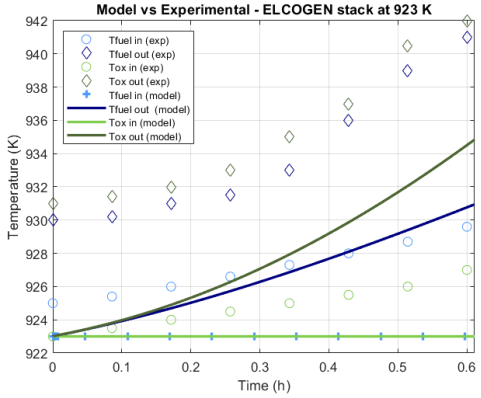


Fig. 6. Comparison between experimental and simulated temperature profiles at the inlet and outlet of the anode and cathode channels of the ELCOGEN stack at 923 K

As shown in Fig. 7, the experimentally measured inlet temperatures T_fuel_in and T_ox_in are directly used as boundary conditions of the thermal model, instead of assuming a constant value equal to the furnace temperature. This allows the model's ability to reproduce the internal heat transfer within the stack to be evaluated independently of the inlet temperature assumption.

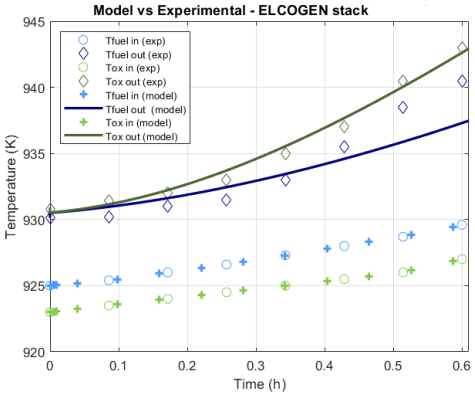


Fig. 7. Validation of the thermal model using experimental inlet temperature boundary conditions for the ELCOGEN stack

Fig. 8 presents the relative error between the simulated and experimental inlet and outlet temperatures of the anode and cathode channels. The relative error remains below 0.3% throughout the current ramp, confirming the accuracy of the proposed thermal model.

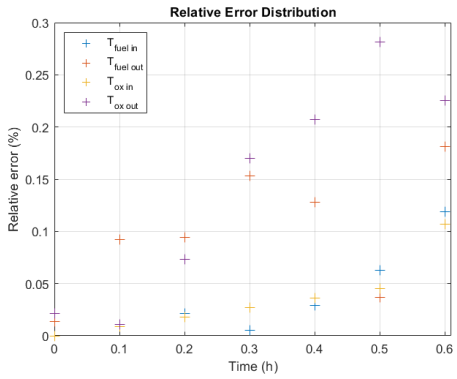


Fig. 8. Relative error between simulated and experimental temperatures at the anode and cathode channel inlets and outlets of the ELCOGEN stack

The temperature distribution of the middle nodes of the equivalent cell inside the stack during the current ramp at 923 K is illustrated in Fig. 9. The results show that the highest temperatures are observed in the anode T_a, electrolyte T_e, and cathode T_c, where the main heat generation sources are located due to electrochemical reactions and associated losses. Intermediate temperatures are observed for the nodes T_4, and T_5, which are located between these main layers and act as thermal transition regions. Lower temperatures are obtained for the nodes T_6 and T_3, situated between the electrodes and the gas channels. The anode and cathode channel temperatures T_{fuel} and T_{ox} are lower due to the cooling effect of the gas flows. Finally, the lowest temperatures are observed at the boundary nodes T_1, T_{i1}, and T_2 on one side, and T_8, T_{i2}, and T_7 on the other side, as these nodes are closer to the external environment and therefore experience higher heat losses.

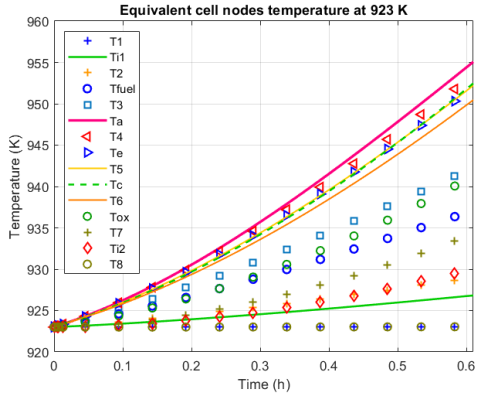


Fig. 9. Temperature evolution of the middle nodes in the anode and cathode channels of the ELCOGEN stack at 923 K

IV. CONCLUSION

In this work, a two-dimensional thermal model of a planar SOFC stack was developed to analyze the temperature distribution within the different stack layers. The results highlighted the main thermal phenomena and identified the most thermally affected regions of the stack. The model was validated against experimental data available in the literature and obtained from the same ELCOGEN E350 stack, showing good agreement between simulations and measurements. This study confirms the relevance of thermal modeling for a better understanding of SOFC stack behavior and represents a first step toward the development of a complete system-level multiphysics model. Future work will focus on sensitivity analysis, extending the proposed thermal model to a multi-cell SOFC stack, and performing dedicated experimental investigations on the real stack to further validate and refine the proposed model.

ACKNOWLEDGMENT

This work was supported by the EIPHI Graduate School (contract ANR-17-EURE-0002), the Bourgogne-Franche-Comté Region. This work was supported by a grant from the French State, managed by the National research Agency under the Investments for the Future program, reference ANR-21-ESRE-0033. and the FLEXISOC project within the PEPR Hydrogen program.

Références

[1] B. van Veldhuizen, B. van, Lindert, A. Vellayani, Purushothaman et K. Visser, «Solid Oxide Fuel Cells for Marine Applications,» *International Journal of Energy Research*, vol. 2023, n°1Article ID 5163448, p. 5163448, 2023.

[2] A. Ashar, L. Wehrle, O. Deutschmann et R. J. Braun, «High performance ammonia-fueled SOFC hybrid system for decarbonizing heavy-duty transportation applications,» *Applied Energy*, vol. 390, n°1C, 2025.

[3] FuelCellsWorks, «HD Hyundai Accelerates Entry Into European Market with Fuel Cell Technology for Cruise Ships,» FuelCellsWorks, 19 Jun 2025. [En ligne]. Available: https://fuelcellsworks.com/2025/06/19/fuel-cells/hd-hyundai-accelerates-entry-into-european-market-with-fuel-cell-technology-for-cruise-ships. [Accès le Jun 2025].

[4] Z. Wu, P. Zhu, Y. Huang, J. Yao, F. Yang, Z. Zhang et M. Ni, «A Comprehensive Review of Modeling of Solid Oxide Fuel Cells: From Large Systems to Fine Electrodes,» *Chemical Reviews (Chem. Rev.)*, vol. 125, p. 2184–2268, 2025.

[5] Elcogen, «Solid oxide stacks for fuel cell systems,» Elcogen, [En ligne]. Available: https://elcogen.com/products/solid-oxide-stacks-for-fuel-cell-systems/.

[6] J. Lesmayoux, « Characterization and Modeling in Static and Dynamic Regimes of an Intermediate Temperature Solid Oxide Fuel Cell Stack (IT-SOFC)» National Polytechnic Institute of Toulouse, INP, Toulouse, France, 2022.

[7] M. Chnani, « Macroscopic Modeling of PEFC and SOFC Fuel Cells for the Study of Their Coupling» University of Franche-Comté / University of Technology of Belfort-Montbéliard, France, 2008..

[8] M. Chnanin, M.-C. Péra, R. Glises, J. Kauffman et D. Hissel, «Transient thermal behaviour of a solid oxide fuel cell,» New York, NY, USA, 2007.

[9] Y. Cengel, Heat Transfer: A Practical Approach,NY 2003.

[10] Q. Xu, L. Xia, Q. He, Z. Guo et M. Ni, «Thermo-electrochemical modelling of high temperature methanol-fuelled solid oxide fuel cells,» *Applied Energy (Appl. Energy)*, vol. 291, p. 116832, 2021.

[11] H. Xu, B. Chen, H. Zhang, W. Kong, B. Liang et M. Ni, «The thermal effect in direct carbon solid oxide fuel cells,» *Applied Thermal Engineering (Appl. Therm. Eng.)*, 2016.

[12] L. Xia, A. Khosravi, M. Han et L. Sun, « Modelica based hybrid-dimensional dynamic modeling, multi-objective optimization and thermodynamic analysis of cross-flow SOFC system,» *Renewable Energy (Renew. Energy)*, vol. 241, n°1122372, 2025.

[13] W. Xia, Y. Yang et Q. Wang, «Effects of operations and structural parameters on the one-cell stack performance of planar solid oxide fuel cell,» *Journal of Power Sources*, vol. 194, n° 12, pp. 886-898, 2009.